

Grounded Hyperspheres as Squashed Wormholes

H Alshal^{1,2*} and T Curtright^{2†}

¹Department of Physics, Cairo University, Giza, 12613, Egypt

²Department of Physics, University of Miami, Coral Gables, FL 33124-8046, USA

5 December 2018

Abstract

We compute exterior Green functions for equipotential, grounded hyperspheres in N -dimensional electrostatics by squashing Riemannian wormholes, where an image charge is placed in the branch of the wormhole opposite the branch containing the source charge, thereby providing a vivid geometrical approach to a method first suggested in 1897 by Sommerfeld. We compare and contrast the strength and location of the image charge in the wormhole approach with that of the conventional Euclidean solution where an image charge of reduced magnitude is located inside the hypersphere. While the two approaches give mathematically equivalent Green functions, we believe they provide strikingly different physics perspectives.

In tribute to Richard Feynman (1918-1988) and Arnold Sommerfeld (1868-1951)

1 Introduction

Feynman constantly emphasized that insight could be gained by approaching a problem from a different point of view [13]. We follow that philosophy here to construct a Green function, G_o , for the N -dimensional electrostatics of an equipotential, grounded hypersphere — i.e. a “conducting” hypersphere. We stress the geometrical aspects of a method first employed in the late 19th century by Sommerfeld [6], albeit not for this specific problem. Although the method was introduced some 120 years ago [15], we believe it suggests insights that are not widely appreciated. While Sommerfeld’s method has been employed during the intervening century to solve a handful of otherwise difficult electrostatic and heat conduction problems [10, 16, 3, 4, 5], we believe that a stronger emphasis on its geometrical aspects is worthwhile and justifies applying the method to a broader class of problems, even those which are not difficult to solve by other means. To that end we reconsider grounded hyperspheres in N *spatial* dimensions.

Although the Green function with homogeneous Dirichlet boundary conditions is known for the grounded hypersphere and can be obtained using well-known techniques, here we compute G_o by a novel method that uses “wormholes” [14, 11] in an N -dimensional Riemannian space. We build appropriate Green functions for the invariant Laplacian, ∇^2 , acting on various wormhole geometries, initially by imposing boundary conditions only asymptotically, to obtain G , and finally by requiring that the Green function also vanish at the narrowest part of the wormhole’s “throat” to obtain G_o .

To be more specific, we consider N -dimensional versions of the isotropic Ellis wormhole [8], whose equatorial slices have radii given by $r(w) = \sqrt{R^2 + w^2}$ where R is a constant and $-\infty \leq w \leq +\infty$. We construct these manifolds so that the region near $w = 0$ is a curved bridge [7] that connects two distinct branches of the manifold, with those branches approaching two separate copies of N -dimensional Euclidean space, \mathbb{E}_N , asymptotically as $w \rightarrow \pm\infty$ (please see the Figures). We build appropriate Green functions for ∇^2 acting on these specific geometries, once again by first imposing boundary conditions only as $w \rightarrow \pm\infty$, to obtain G , and then by requiring that the Green function also vanish at $w = 0$, i.e. at radius R , to obtain G_o .

*alshal@cu.edu.eg

†curtright@miami.edu

The “grounded” Green function G_o is constructed by placing a source and its negative image at exactly the *same radius* and in precisely the *same direction* on the manifold, but on *opposite* branches — somewhat striking but nevertheless very natural positions in this context.

Next we introduce deformations of the Ellis wormhole whose radii are given by the p -norm $r(w) = (R^p + |w|^p)^{1/p}$. We compute Green functions G and G_o for this family of manifolds as well. Finally, we consider the $p \rightarrow 1$ limit of this family of manifolds and Green functions.

In the $p \rightarrow 1$ limit, where $r(w) = R + |w|$ is the so-called Manhattan norm, both branches of the manifold are completely “squashed flat”. That is to say, the manifold degenerates into two distinct Euclidean spaces joined together along a hyperspherical “doorway” of radius R . (For equatorial slices of the manifolds as p approaches 1, please see the Figures.) However, the *interior* of the hypersphere is *excluded* from either branch. Moreover, in this limit it is clear that by restricting G_o to have source and field points on just one of the distinct branches, a Green function for the grounded equipotential hypersphere is obtained. Minor rearrangements of the terms shows that G_o is in exact agreement with the usual symmetrized Green function for the grounded hypersphere, as obtained by considering a single copy of \mathbb{E}_N with an image charge placed inside the hypersphere.

2 Electrostatics in N Euclidean dimensions

The point-particle electric potential in an N -dimensional Euclidean space, \mathbb{E}_N , is well-known to vary inversely with distance as the $(N - 2)$ -th power. For a unit point charge located at the origin,

$$\Phi_{\mathbb{E}_N}(\vec{r}) = \frac{k_N}{r^{N-2}}, \quad \nabla^2 \Phi_{\mathbb{E}_N}(\vec{r}) = -\delta^N(\vec{r}), \quad k_N \equiv \frac{1}{(N-2)\Omega_N} \quad (1)$$

The total hyper-angle Ω_N (i.e. the area of the *unit radius* sphere, S_{N-1} , embedded in N dimensions) is given by

$$\Omega_N = \int_{S_{N-1}} d\Omega = \frac{2\pi^{N/2}}{\Gamma(N/2)}. \quad (2)$$

where $d\Omega$ is the standard measure on S_{N-1} . For example, $\Omega_1 = 2$, $\Omega_2 = 2\pi$, $\Omega_3 = 4\pi$, $\Omega_4 = 2\pi^2$, etc. The case $N = 2$ is handled as a limit, to obtain

$$\Phi_{\mathbb{E}_2}(\vec{r}) = -\frac{1}{2\pi} \ln(r/R), \quad \nabla^2 \Phi_{\mathbb{E}_2}(\vec{r}) = -\delta^2(\vec{r}), \quad (3)$$

up to a constant R that sets the distance scale. For more details in this particular case, see [2].

Consequently, a Green function for \mathbb{E}_N is

$$G_{\mathbb{E}_N}(\vec{r}_1; \vec{r}_2) = \frac{k_N}{|\vec{r}_1 - \vec{r}_2|^{N-2}}, \quad \nabla^2 G_{\mathbb{E}_N}(\vec{r}_1; \vec{r}_2) = -\delta^N(\vec{r}_1 - \vec{r}_2) \quad (4)$$

This result is translationally invariant, that is to say, $G_{\mathbb{E}_N}(\vec{r}_1; \vec{r}_2)$ depends only on the difference $\vec{r}_1 - \vec{r}_2$. Moreover, this choice for the Green function incorporates boundary conditions at spatial infinity that mimic the behavior in (1). So any sufficiently localized charge distribution $\rho(\vec{r})$ gives rise to the usual linear superposition,

$$\Phi(\vec{r}_1) = \int G_{\mathbb{E}_N}(\vec{r}_1; \vec{r}_2) \rho(\vec{r}_2) d^N r_2 \quad (5)$$

where we assume the integral is well-defined and finite. For a localized charge distribution, $\Phi(\vec{r}_1) \underset{r_1 \rightarrow \infty}{\sim} \frac{k_N Q}{r_1^{N-2}} + O\left(\frac{1}{r_1^{N-1}}\right)$ where $Q = \int \rho(\vec{r}_2) d^2 r_2$ is the total charge. Finally, we note that the Green function (4) in N dimensions can be expanded in terms of Gegenbauer polynomials, $C_l^{(\alpha)}(\cos \theta)$, namely,

$$\frac{1}{|\vec{r}_1 - \vec{r}_2|^{N-2}} = \sum_{l=0}^{\infty} \frac{(r_<)^l}{(r_>)^{l+N-2}} C_l^{(\frac{N-2}{2})}(\hat{r}_1 \cdot \hat{r}_2) \quad (6)$$

where $\hat{r}_1 \cdot \hat{r}_2 \equiv \cos \theta$ and $r_>$ or $r_<$ is the max or min of r_1 and r_2 , respectively. This is a straightforward generalization of the well-known $N = 3$ case that involves the Legendre polynomials $P_l(\cos \theta)$.

3 Electrostatics in N curved dimensions

On a Riemannian manifold, described by a metric $g_{\mu\nu}$, distance increments are given by ds where

$$(ds)^2 = g_{\mu\nu} dx^\mu dx^\nu \quad (7)$$

Summation over integer μ and ν is implicitly understood, with $1 \leq \mu, \nu \leq N$ for an N -dimensional manifold. The invariant Laplacian on such a manifold is given by

$$\nabla^2 = \frac{1}{\sqrt{g}} \partial_\mu (\sqrt{g} g^{\mu\nu} \partial_\nu) \quad (8)$$

where $g \equiv \det g_{\mu\nu}$ and $g^{\mu\nu}$ is the matrix inverse of $g_{\mu\nu}$.

Consider now an infinite isotropic manifold with

$$(ds)^2 = (dw)^2 + r^2(w) (d\hat{r})^2 \quad (9)$$

The variable w takes on values $-\infty \leq w \leq +\infty$, the unit vectors \hat{r} represent the points on S_{N-1} in terms of the standard angular parameterization, and $r(w)$ is assumed to be a positive, non-vanishing “radius” function that has a minimum at $w = 0$ and becomes infinite as $w \rightarrow \pm\infty$. For fixed angles, radial displacements on the manifold are determined just by $ds = \pm dw$.

We refer to $w > 0$ and $w < 0$ as the “upper” and “lower” branches of the manifold, respectively, and following Einstein and Rosen [7], we call the region near $w = 0$ the “bridge” between the two branches. For visualization purposes, please see the examples shown in the Figures.

The metric, its inverse, and the determinant g have well-known, standard expressions for this manifold. In any case, the form of the metric leads to the invariant Laplacian

$$\nabla^2 = \frac{1}{r(w)^{N-1}} \partial_w \left(r(w)^{N-1} \partial_w \right) - \frac{1}{r(w)^2} L^2, \quad (10)$$

where all the $N-1$ angular derivatives are contained in $L_{jk} \equiv -i(x_j \partial_k - x_k \partial_j)$ with $L^2 \equiv \sum_{1 \leq j < k \leq N} L_{jk} L_{jk}$.

The eigenfunctions of L^2 form a complete set on S_{N-1} , the hyperspherical harmonics $Y_{lm_1 m_2 \dots m_{N-2}}$, analogous to the familiar spherical harmonics Y_{lm} on S_2 . The $Y_{lm_1 m_2 \dots m_{N-2}}$ depend on the $N-1$ angles parameterizing all points on the hypersphere, but do not depend on w . Thus, with unit vectors \hat{r}_1 and \hat{r}_2 representing two points on S_{N-1} ,

$$\sum_{l, m_1, m_2, \dots, m_{N-2}} Y_{lm_1 m_2 \dots m_{N-2}}(\hat{r}_1) Y_{lm_1 m_2 \dots m_{N-2}}^*(\hat{r}_2) = \delta^{N-1}(\hat{r}_1 - \hat{r}_2), \quad \int \delta^{N-1}(\hat{r}_1 - \hat{r}_2) d\Omega(\hat{r}_1) = 1 \quad (11)$$

More details about hyperspherical harmonics may be found in various books, although notation and conventions may differ from those used here. Acting on $Y_{lm_1 m_2 \dots m_{N-2}}$ the L^2 eigenvalues are given by

$$L^2 Y_{lm_1 m_2 \dots m_{N-2}} = l(l + N - 2) Y_{lm_1 m_2 \dots m_{N-2}} \quad (12)$$

for $l = 0, 1, 2, \dots$, generalizing the well-known $N = 3$ case. As a further generalization of $N = 3$ results, there is an addition formula for hyperspherical harmonics resulting in a Gegenbauer polynomial. For fixed l in N dimensions,

$$\frac{2l + N - 2}{N - 2} C_l^{\left(\frac{N-2}{2}\right)}(\hat{r}_1 \cdot \hat{r}_2) = \Omega_N \sum_{m_1, m_2, \dots, m_{N-2}} Y_{lm_1 m_2 \dots m_{N-2}}(\hat{r}_1) Y_{lm_1 m_2 \dots m_{N-2}}^*(\hat{r}_2) \quad (13)$$

where our orthonormalization convention is

$$\int Y_{lm_1 \dots m_{N-2}}(\hat{r}) Y_{l'm'_1 \dots m'_{N-2}}^*(\hat{r}) d\Omega = \delta_{ll'} \delta_{m_1 m'_1} \dots \delta_{m_{N-2} m'_{N-2}} \quad (14)$$

Elementary harmonic functions on the manifold have the form

$$h_{lm_1m_2\cdots m_{N-2}} = h_l(w) Y_{lm_1m_2\cdots m_{N-2}}(\hat{r}) \quad (15)$$

where the radial functions satisfy the equation

$$\frac{l(l+N-2)}{r(w)^2} h_l(w) = \frac{1}{r(w)^{N-1}} \frac{d}{dw} \left(r(w)^{N-1} \frac{d}{dw} h_l(w) \right) \quad (16)$$

$$= \frac{1}{r(w)} \frac{d}{dw} \left(r(w) \frac{d}{dw} h_l(w) \right) + (N-2) \frac{r'(w)}{r(w)} \frac{d}{dw} h_l(w) \quad (17)$$

Suppose $h_l^{(1)}$ and $h_l^{(2)}$ are two solutions of this second-order differential equation. Then by Abel's identity their Wronskian is

$$W[h_l^{(1)}(w), h_l^{(2)}(w)] \equiv h_l^{(1)}(w) \overleftrightarrow{\frac{d}{dw}} h_l^{(2)}(w) = \frac{c_l}{r^{N-1}(w)} \quad (18)$$

where $c_l = r^{N-1}(0) W[h_l^{(1)}(0), h_l^{(2)}(0)]$ is a constant. For the cases of interest, $r(w)$ is monotonic in $|w|$ as well as symmetric under $w \rightarrow -w$, and therefore if $h_l(w)$ is a solution to (16), so is $h_l(-w)$.

For the rest of the discussion, we assume both $r(w) = r(-w)$ and $r(w) \underset{w \rightarrow \pm\infty}{\sim} |w|$, in which case the asymptotic behavior of the two radial functions is familiar¹ since to leading order (16) reduces to

$$\frac{1}{|w|^{N-1}} \frac{d}{dw} \left(|w|^{N-1} \frac{d}{dw} h_l(w) \right) \underset{r \rightarrow \pm\infty}{\sim} \frac{l(l+N-2)}{|w|^2} h_l(w) \quad (19)$$

with simple power law solutions

$$h_l(w) \underset{w \rightarrow \pm\infty}{\sim} |w|^l \quad \text{or} \quad \frac{1}{|w|^{l+N-2}} \quad (20)$$

For $N > 2$ we identify the exact solution that falls off when $w \rightarrow +\infty$ but does not fall off when $w \rightarrow -\infty$ as $h_l^{(+)}$. Thus, with a normalization chosen for convenience,

$$h_l^{(+)}(w) \underset{w \rightarrow +\infty}{\sim} \frac{1}{|w|^{l+N-2}}, \quad h_l^{(+)}(w) \underset{w \rightarrow -\infty}{\sim} b_l |w|^l \quad (21)$$

where b_l is another constant. For the cases of interest, for which $r(w) = r(-w)$, it follows that $h_l^{(-)}(w) \equiv h_l^{(+)}(-w)$ is an independent exact solution that has the asymptotic behavior

$$h_l^{(-)}(w) \underset{w \rightarrow -\infty}{\sim} \frac{1}{|w|^{l+N-2}}, \quad h_l^{(-)}(w) \underset{w \rightarrow +\infty}{\sim} b_l |w|^l \quad (22)$$

Independence follows from the Wronskian

$$\begin{aligned} W[h_l^{(-)}(w), h_l^{(+)}(w)] &\equiv h_l^{(-)}(w) \overleftrightarrow{\frac{d}{dw}} h_l^{(+)}(w) \underset{w \rightarrow +\infty}{\sim} b_l \left(w^l \frac{(-l-N+2)}{w^{l+N-1}} - \frac{1}{w^{l+N-2}} w^{l-1} l \right) \\ &\underset{w \rightarrow +\infty}{\sim} b_l \frac{(2-N-2l)}{w^{N-1}} \end{aligned} \quad (23)$$

as expected from the asymptotic form of (18) with $c_l = (2-N-2l)b_l$.

For $N > 2$ then, a Green function that vanishes as $|w| \rightarrow \infty$ has the form

$$\begin{aligned} G(w_1, \hat{r}_1; w_2, \hat{r}_2) &= \sum_{l, m_1, m_2, \dots, m_{N-2}} \frac{1}{c_l} h_l^{(+)}(w_>) h_l^{(-)}(w_<) Y_{lm_1m_2\cdots m_{N-2}}(\hat{r}_1) Y_{lm_1m_2\cdots m_{N-2}}^*(\hat{r}_2) \\ &= \frac{1}{(2-N)\Omega_N} \sum_{l=0}^{\infty} \frac{1}{b_l} h_l^{(+)}(w_>) h_l^{(-)}(w_<) C_l^{\left(\frac{N-2}{2}\right)}(\cos\theta) \end{aligned} \quad (24)$$

¹Compare (19) to the usual radial equation and its solutions on \mathbb{E}_N , namely, $\frac{1}{r^{N-1}} \frac{d}{dr} \left(r^{N-1} \frac{d}{dr} h_l(r) \right) = \frac{l(l+N-2)}{r^2} h_l(r)$, which is solved by $h_l(r) = C_1 r^l + C_2 r^{2-N-l}$.

where $w_>$ or $w_<$ is the max or min of w_1 and w_2 , respectively. When $r(w) = r(-w)$ it follows that

$$G(w_1, \hat{r}_1; w_2, \hat{r}_2) = G(w_2, \hat{r}_2; w_1, \hat{r}_1) \quad (25)$$

and, due to the isotropy of the manifold, the sum over the various m_k labeling the hyperspherical harmonics always reduces to a function of just a single angle θ , namely, $C_l^{(\frac{N-2}{2})}(\cos \theta)$ with $\cos \theta \equiv \hat{r}_1 \cdot \hat{r}_2$.

Completeness of the $Y_{lm_1 m_2 \dots m_{N-2}}$ on the hypersphere S_{N-1} and the radial discontinuity given by

$$\lim_{\varepsilon \rightarrow 0} \frac{d}{dw_1} \left(r(w_1)^{N-1} h_l^{(+)}(w_1) \right) h_l^{(-)}(w_2) \Big|_{w_1=w_2+\varepsilon} - \lim_{\varepsilon \rightarrow 0} h_l^{(+)}(w_2) \frac{d}{dw_1} \left(r(w_1)^{N-1} h_l^{(-)}(w_1) \right) \Big|_{w_1=w_2-\varepsilon} = -c_l \quad (26)$$

produces the expected invariant Dirac delta in the equation obeyed by G , namely,

$$\nabla^2 G(w_1, \hat{r}_1; w_2, \hat{r}_2) = -\frac{1}{r(w)^{N-1}} \delta(w_1 - w_2) \delta^{N-1}(\hat{r}_1 - \hat{r}_2) \quad (27)$$

If either $w_> \rightarrow +\infty$ or $w_< \rightarrow -\infty$, the individual terms vanish in the sum (24), so that the Green function satisfies the homogeneous boundary condition $G = 0$, assuming convergence of the sum. However, when $w_2 = 0$ the value of G is not so obvious. Nevertheless, a simple linear combination can be selected to construct a Green function that vanishes at $w_2 = 0$, namely,

$$G_o(w_1, \hat{r}_1; w_2, \hat{r}_2) = G(w_1, \hat{r}_1; w_2, \hat{r}_2) - G(w_1, \hat{r}_1; -w_2, \hat{r}_2) \quad (28)$$

Note that G_o is manifestly an odd function of w_2 and is also an odd function of w_1 as a consequence of (25).

This G_o has a simple interpretation as the potential at (w_1, \hat{r}_1) due to a point charge source at (w_2, \hat{r}_2) and a negative image charge of that point source at $(-w_2, \hat{r}_2)$. The source and image charges are therefore of *equal* magnitude but opposite sign, and are positioned symmetrically but on *opposite* branches of the manifold. So, if both w_1 and w_2 are restricted to one branch of the manifold, (27) will still hold on that branch, since the image will produce an additional Dirac delta only on the other branch. Therefore G_o is an appropriate Green function to solve $\nabla^2 \Phi = -\rho$ on the upper branch of the manifold with the condition $\Phi = 0$ on the inner boundary of that branch, i.e. on the hypersphere at $w = 0$.

The radial equation (16) is perhaps more transparent after changing variable to

$$u = \int_0^w \frac{d\varpi}{r(\varpi)} \quad (29)$$

with implicit inverse $w(u)$. Note that $\text{sgn } u = \text{sgn } w$, and if $r(w) \underset{w \rightarrow \pm\infty}{\sim} |w|$ then $u \underset{w \rightarrow \pm\infty}{\rightarrow} \pm\infty$. With this variable change, the radial parts of harmonic functions satisfy the equation

$$\frac{d^2}{du^2} h_l + (N-2) r'(w(u)) \frac{d}{du} h_l = l(l+N-2) h_l \quad (30)$$

This may be cast into Sturm-Liouville form on the interval $-1 \leq t \leq +1$ upon changing variables to $t = \tanh u$, and multiplying by the integrating factor

$$\mu(t) = \exp \left(\int_0^t \frac{(N-2) r'(w(\arctanh \tau))}{(1-\tau^2)} d\tau \right) \quad (31)$$

The result is

$$\frac{d}{dt} \left(\mu(t) (1-t^2) \frac{d}{dt} h_l \right) = \frac{l(l+N-2)}{1-t^2} \mu(t) h_l \quad (32)$$

So written, the reader can easily find in the mathematical literature several detailed discussions of Green functions for this equation.

4 The Ellis wormhole in N dimensions

The so-called Ellis wormhole [8] is defined by (9) with

$$r(w) = \sqrt{R^2 + w^2} \quad (33)$$

or $w = \pm\sqrt{r^2 - R^2}$ on the upper and lower branches of the wormhole, respectively. In this case

$$u(w) = \int_0^w \frac{dv}{\sqrt{R^2 + v^2}} = \operatorname{arcsinh}\left(\frac{w}{R}\right) = \ln\left(\frac{w}{R} + \sqrt{1 + \frac{w^2}{R^2}}\right) \quad (34)$$

$$w(u) = R \sinh u, \quad r(w(u)) = R \cosh u, \quad r'(w(u)) = \frac{w(u)}{\sqrt{R^2 + w^2(u)}} = \tanh u \quad (35)$$

and therefore

$$\frac{d^2}{du^2} h_l + (N-2)(\tanh u) \frac{d}{du} h_l = l(l+N-2) h_l \quad (36)$$

This has exact solutions

$$h_l^{(1)}(u) = \frac{(1 + \tanh u)^{\frac{1}{2}(N+l-2)}}{(1 - \tanh u)^{\frac{1}{2}l}} {}_2F_1\left(2 - \frac{1}{2}N, \frac{1}{2}N - 1; 2 - \frac{1}{2}N - l; \frac{1 - \tanh u}{2}\right) \quad (37)$$

$$h_l^{(2)}(u) = \frac{(1 - \tanh u)^{\frac{1}{2}(N+l-2)}}{(1 + \tanh u)^{\frac{1}{2}l}} {}_2F_1\left(2 - \frac{1}{2}N, \frac{1}{2}N - 1; \frac{1}{2}N + l; \frac{1 - \tanh u}{2}\right) \quad (38)$$

when written in terms of Gauss hypergeometric functions,

$${}_2F_1(a, b; c; z) = \sum_{k=0}^{\infty} \frac{(a)_k (b)_k}{(c)_k} \frac{z^k}{k!} \quad (39)$$

where $(a)_k = \Gamma(a+k)/\Gamma(a)$, etc. It follows that $h_l^{(1)}$ is well-behaved as $u \rightarrow -\infty$ for all even $N > 2$, but *not* for odd N , where it is necessary to take a linear combination of $h_l^{(1)}$ and $h_l^{(2)}$ to find good behavior. On the other hand, $h_l^{(2)}$ is well-behaved as $u \rightarrow +\infty$ for all $N > 2$. (For $N = 2$, see [2].)

Evidently the simplest case beyond two dimensions is $N = 4$, for which the general solution of (36) is given by

$$h_l(u) = \frac{1}{\cosh u} (c_1 \exp[(l+1)u] + c_2 \exp[-(l+1)u]) \quad (40)$$

for any constants c_1 and c_2 . That is to say,

$$h_l^{(1,2)}(u) = \frac{1}{\cosh u} \exp[\pm(l+1)u], \quad h_l^{(1)}(-\infty) = 0, \quad h_l^{(2)}(+\infty) = 0 \quad (41)$$

$$W[h_l^{(1)}(u), h_l^{(2)}(u)] \equiv h_l^{(1)}(u) \overleftrightarrow{\frac{d}{du}} h_l^{(2)}(u) = -\frac{2(l+1)}{\cosh^2 u} \quad (42)$$

Or, in terms of the variable $t = \tanh u = \frac{w}{\sqrt{R^2 + w^2}}$, for $N = 4$ the two independent solutions (37) and (38) become

$$h_l^{(1,2)}(t) = \frac{(1 \pm t)^{l+1}}{(1 - t^2)^{l/2}}, \quad h_l^{(1)}(-1) = 0, \quad h_l^{(2)}(+1) = 0 \quad (43)$$

$$W[h_l^{(1)}(t), h_l^{(2)}(t)] \equiv h_l^{(1)}(t) \overleftrightarrow{\frac{d}{dt}} h_l^{(2)}(t) = -2(l+1) \quad (44)$$

In terms of these harmonic functions for $N = 4$, the Green function (24) is

$$\begin{aligned}
G(w_1, \hat{r}_1; w_2, \hat{r}_2) &= \frac{1}{4\pi^2 \sqrt{(R^2 + w_1^2)(R^2 + w_2^2)}} \sum_{l=0}^{\infty} \left(\sqrt{\frac{(w_1 + \sqrt{R^2 + w_1^2})(w_2 - \sqrt{R^2 + w_2^2})}{(w_1 - \sqrt{R^2 + w_1^2})(w_2 + \sqrt{R^2 + w_2^2})}} \right)^{l+1} C_l^{(1)}(\hat{r}_1 \cdot \hat{r}_2) \\
&= \frac{1}{4\pi^2 \sqrt{(R^2 + w_1^2)(R^2 + w_2^2)}} \frac{1}{\sqrt{\frac{(w_1 + \sqrt{R^2 + w_1^2})(w_2 - \sqrt{R^2 + w_2^2})}{(w_1 - \sqrt{R^2 + w_1^2})(w_2 + \sqrt{R^2 + w_2^2})}} + \sqrt{\frac{(w_1 - \sqrt{R^2 + w_1^2})(w_2 + \sqrt{R^2 + w_2^2})}{(w_1 + \sqrt{R^2 + w_1^2})(w_2 - \sqrt{R^2 + w_2^2})}} - 2\hat{r}_1 \cdot \hat{r}_2}
\end{aligned} \tag{45}$$

In the last line we have used the sum

$$\sum_{l=0}^{\infty} x^l C_l^{(1)}(\cos \theta) = \frac{1}{1 + x^2 - 2x \cos \theta} \tag{46}$$

This result for the $N = 4$ Green function is more compactly written as

$$G(w_1, \hat{r}_1; w_2, \hat{r}_2) = \frac{1}{4\pi^2 r_1 r_2 \left(\sqrt{\frac{(r_1 + w_1)(r_2 - w_2)}{(r_1 - w_1)(r_2 + w_2)}} + \sqrt{\frac{(r_2 + w_2)(r_1 - w_1)}{(r_1 + w_1)(r_2 - w_2)}} - 2\hat{r}_1 \cdot \hat{r}_2 \right)} \tag{47}$$

where $r_1 \equiv \sqrt{R^2 + w_1^2}$ and $r_2 \equiv \sqrt{R^2 + w_2^2}$. Note that $G(w_1, \hat{r}_1; w_2, \hat{r}_2) = G(w_2, \hat{r}_2; w_1, \hat{r}_1)$. The $N = 4$ Green function for the grounded wormhole is then defined as in (28), so that $G_o(w_1, \hat{r}_1; w_2, \hat{r}_2) = -G_o(-w_1, \hat{r}_1; w_2, \hat{r}_2)$.

Asymptotically, with both points on the upper branch of the manifold,

$$G(w_1, \hat{r}_1; w_2, \hat{r}_2) \underset{w_1, w_2 \gg R}{\sim} \frac{1}{4\pi^2 |\vec{r}_1 - \vec{r}_2|^2} + O\left(\frac{R}{r_{1,2}^3}\right) \tag{48}$$

As should be expected, the leading term here is in agreement with (4) for $N = 4$.

A contour plot of G versus w_1 and $\theta \equiv \arccos(\hat{r}_1 \cdot \hat{r}_2)$ is shown for the $N = 4$ Ellis wormhole in Figure 10, with $R = 1$ and unit source at $(w_2, \hat{r}_2) = (1, \hat{r}_2)$. A similar plot of G_o versus w_1 and θ is shown in Figure 11. In addition to the unit source at $(w_2, \hat{r}_2) = (1, \hat{r}_2)$, G_o incorporates a negative image of that source at $(w_2, \hat{r}_2) = (-1, \hat{r}_2)$.

5 The p -norm wormholes

Consider next a continuous deformation of the Ellis wormhole. Define a class of “ p -norm radial functions” with R a constant radius, $p \geq 1$ a real number, and

$$r(w) = (R^p + |w|^p)^{1/p} \tag{49}$$

Note that indeed $r(w) \underset{|w| \gg R}{\sim} |w|$, so the asymptotic behavior of harmonic functions on these manifolds falls within the scope of the discussion following (19). Also note the case $p = 2$ is the Ellis wormhole. Equatorial slices of the manifolds defined by (49) and (9) for various values of p are shown in the Figures as 3D embeddings of 2D surfaces, to obtain curved surfaces of revolution about the z -axis.

As $p \rightarrow 1$, or else as $p \rightarrow \infty$, this class of manifolds continuously interpolates between the Ellis wormhole, with its smoothly curved bridge, and two flattened copies of \mathbb{E}_N each of which is missing an N -ball \mathbb{B}_N of radius R . That is to say, varying p away from $p = 2$ interpolates between the Ellis wormhole and a pair of $\mathbb{E}_N - \mathbb{B}_N(R)$ manifolds, either as $p \rightarrow 1$ or else as $p \rightarrow \infty$. Nonetheless, the two copies of $\mathbb{E}_N - \mathbb{B}_N(R)$ are joined together, either by a single S_{N-1} of radius R , as $p \rightarrow 1$, or by a tube composed of such S_{N-1} s, as $p \rightarrow \infty$. For the first of these limits, we say the two copies of $\mathbb{E}_N - \mathbb{B}_N(R)$ are “creased” together on a

single hypersphere of radius R , that hypersphere providing an open “doorway” to go from one copy of $\mathbb{E}_N - \mathbb{B}_N(R)$ to the other.

For G and G_o , in this short section on generic p -norm manifolds we are content to refer to the previous general discussion of the Green functions. To supplement that discussion, we only point out that the variable u defined in (29) is explicitly given for the p -norm radial functions by Gauss hypergeometric functions, namely,

$$u(w) = \int_0^w \frac{1}{(R^p + (\varpi^2)^{p/2})^{1/p}} d\varpi = \frac{w}{R} {}_2F_1\left(\frac{1}{p}, \frac{1}{p}; 1 + \frac{1}{p}; -\left(\frac{w^2}{R^2}\right)^{\frac{1}{2}p}\right) \quad (50)$$

6 The squashed wormhole and its Green functions

Flattening the two branches of the wormhole, to obtain two independent copies of $\mathbb{E}_N - \mathbb{B}_N(R)$ joined together on a common hypersphere, is achieved by taking the $p = 1$ Manhattan norm.²

$$r(w) = R + |w| \quad (51)$$

Then so long as $w \neq 0$ (16) is solved by familiar functions,

$$h_l(w) = r(w)^l \quad \text{or} \quad r(w)^{2-N-l} \quad (52)$$

It suffices to consider two situations for the source and field point locations, either with w_1 and w_2 on the same branch of the manifold, or with w_1 and w_2 on opposite branches.

Suppose $w_>$ is always on the upper branch, say. Then (24) will have different forms for the two possible source and field point locations.

$$G(w_1, \hat{r}_1; w_2, \hat{r}_2) = k_N \sum_{l=0}^{\infty} \frac{(r(w_<))^l}{(r(w_>))^{l+N-2}} C_l^{(\frac{N-2}{2})}(\hat{r}_1 \cdot \hat{r}_2) \quad \text{if both } w_> > 0 \text{ \& } w_< > 0 \quad (53)$$

$$= k_N \sum_{l=0}^{\infty} \frac{(R)^{2l+N-2}}{(r(w_>)r(w_<))^{l+N-2}} C_l^{(\frac{N-2}{2})}(\hat{r}_1 \cdot \hat{r}_2) \quad \text{if } w_> > 0 \text{ but } w_< < 0 \quad (54)$$

The two forms are chosen so that $G \rightarrow 0$ as $w_> \rightarrow +\infty$ or as $w_< \rightarrow -\infty$, and so that G is continuous as $w_< \rightarrow 0$, i.e. at $r(w_<) = R$.

For the first situation with $w_1 > 0$ and $w_2 > 0$, in light of (6) the sum in (53) gives

$$G(w_1, \hat{r}_1; w_2, \hat{r}_2)|_{\substack{w_1 > 0 \\ w_2 > 0}} = \frac{k_N}{(r^2(w_1) + r^2(w_2) - 2r(w_1)r(w_2)\hat{r}_1 \cdot \hat{r}_2)^{\frac{N-2}{2}}} \quad (55)$$

$$= \frac{k_N}{|\vec{r}_1 - \vec{r}_2|^{N-2}} \quad (56)$$

where in the last expression we have identified $\vec{r}_1 = (R + |w_1|)\hat{r}_1$ and $\vec{r}_2 = (R + |w_2|)\hat{r}_2$ to obtain a symmetrical form that can also be used if both $w_1 < 0$ and $w_2 < 0$.

For the second situation with $w_1 > 0$ and $w_2 < 0$, the sum in (54) gives

$$G(w_1, \hat{r}_1; w_2, \hat{r}_2)|_{\substack{w_1 > 0 \\ w_2 < 0}} = \frac{R^{N-2}k_N}{(r^2(w_1)r^2(w_2) + R^4 - 2R^2r(w_1)r(w_2)\hat{r}_1 \cdot \hat{r}_2)^{\frac{N-2}{2}}} \quad (57)$$

$$= \frac{R^{N-2}k_N}{(r_1^2r_2^2 + R^4 - 2R^2\vec{r}_1 \cdot \vec{r}_2)^{\frac{N-2}{2}}} \quad (58)$$

where in the last expression we have again identified $\vec{r}_1 = (R + |w_1|)\hat{r}_1$ and $\vec{r}_2 = (R + |w_2|)\hat{r}_2$ to obtain a symmetrical form that can also be used if $w_1 < 0$ and $w_2 > 0$.

²In the opposite extreme, when $p \rightarrow \infty$ an equatorial slice of the p -norm wormhole becomes the right-circular cylindrical tube of [11], p 488, Eqn (3).

So, as might have been anticipated, $G(w_1, \hat{r}_1; w_2, \hat{r}_2) = G(w_2, \hat{r}_2; w_1, \hat{r}_1)$ in all situations. Taken together, (55) and (57) give G as a solution to (27) for any field and source point locations on the squashed manifold. A contour plot of G versus w_1 and $\theta \equiv \arccos(\hat{r}_1 \cdot \hat{r}_2)$ is shown for the squashed wormhole in Figure 12, with $N = 4$, $R = 1$, and unit source at $(w_2, \hat{r}_2) = (1, \hat{r}_2)$.

Once again a simple linear combination can be taken to construct a Green function that vanishes at $w_2 = 0$, as in (28). Given that $r(w) = r(-w)$, when both $w_1 > 0$ and $w_2 > 0$ this grounded Green function for the squashed wormhole is explicitly

$$G_o(w_1, \hat{r}_1; w_2, \hat{r}_2)|_{\substack{w_1 > 0 \\ w_2 > 0}} = \frac{k_N}{|\vec{r}_1 - \vec{r}_2|^{N-2}} - \frac{R^{N-2}k_N}{(r_1^2 r_2^2 + R^4 - 2R^2 \vec{r}_1 \cdot \vec{r}_2)^{\frac{N-2}{2}}} \quad (59)$$

Recall that G_o is not only manifestly an odd function of w_2 but is also an odd function of w_1 as a consequence of (28) and the symmetry $G(w_1, \hat{r}_1; w_2, \hat{r}_2) = G(w_2, \hat{r}_2; w_1, \hat{r}_1)$. Therefore, when the field point is on the lower branch of the squashed wormhole with the source on the upper branch,

$$G_o(w_1, \hat{r}_1; w_2, \hat{r}_2)|_{\substack{w_1 < 0 \\ w_2 > 0}} = -\frac{k_N}{|\vec{r}_1 - \vec{r}_2|^{N-2}} + \frac{R^{N-2}k_N}{(r_1^2 r_2^2 + R^4 - 2R^2 \vec{r}_1 \cdot \vec{r}_2)^{\frac{N-2}{2}}} \quad (60)$$

Again, for emphasis, this G_o has the interpretation as the potential at (w_1, \hat{r}_1) due to a point charge source at (w_2, \hat{r}_2) and a negative image charge of that point source at $(-w_2, \hat{r}_2)$. The source and image charges are therefore of *equal* magnitude but opposite sign, and are positioned in an *natural* way on *opposite* branches of the manifold.

At the risk of being repetitive, if both w_1 and w_2 are restricted to one branch of the manifold, (27) will still hold on that branch, since the image will produce an additional Dirac delta only on the other branch. Therefore G_o is an appropriate Green function to solve $\nabla^2 \Phi = -\rho$ on the upper branch of the manifold with the condition $\Phi = 0$ on the inner boundary of that branch, i.e. on the hypersphere at $w = 0$.

When both field and source points are on the upper branch of the wormhole, this result for G_o is exactly the usual result for the Green function in the region exterior to a grounded hypersphere, as obtained by considering only *one copy* of \mathbb{E}_N and putting a unit source at \vec{r}_2 outside the hypersphere along with a negative image source of *reduced strength* $-(R/r_2)^{N-2}$ at an “inversion point” $\vec{r}_{\text{image}} = \frac{R^2}{r_2^2} \vec{r}_2$ that lies *inside* the hypersphere, namely,

$$G_0(\vec{r}_1; \vec{r}_2) = \frac{k_N}{|\vec{r}_1 - \vec{r}_2|^{N-2}} - \frac{R^{N-2}}{r_2^{N-2}} \frac{k_N}{\left|\vec{r}_1 - \frac{R^2}{r_2^2} \vec{r}_2\right|^{N-2}} = G_0(\vec{r}_2; \vec{r}_1) \quad (61)$$

Thus, either image procedure gives the same G_o Green function when restricted to this single copy of $\mathbb{E}_N - \mathbb{B}_N(R)$. In particular, for $N = 4$, on the upper branch of the wormhole,

$$G_0(\vec{r}_1, \vec{r}_2) = \frac{1}{4\pi^2 |\vec{r}_1 - \vec{r}_2|^2} - \frac{R^2}{r_2^2} \frac{1}{4\pi^2 \left|\vec{r}_1 - \frac{R^2}{r_2^2} \vec{r}_2\right|^2} = \frac{1}{4\pi^2 (r_1^2 + r_2^2 - 2\vec{r}_1 \cdot \vec{r}_2)} - \frac{R^2}{4\pi^2 (r_1^2 r_2^2 + R^4 - 2R^2 \vec{r}_1 \cdot \vec{r}_2)} \quad (62)$$

A contour plot of G_o for the $N = 4$ squashed wormhole is shown in Figure 13, for \vec{r}_1 on both upper and lower branches, with a unit source on the upper branch at $(w_2, \theta_2) = (1, 0)$ and its negative image on the lower branch at $(-w_2, \theta_2) = (-1, 0)$.

7 Relating image charge distributions by inversion

Coordinate inversion for a single copy of \mathbb{E}_N maps the interior of the hypersphere to the exterior, and vice versa, and therefore inversion should be expected to relate the standard image method, where the so-called Kelvin image is placed inside the hypersphere, to the Sommerfeld method for the squashed wormhole. Indeed, inversion of the source position is the technique that is normally invoked to locate Kelvin images for grounded hypersphere Green functions on \mathbb{E}_N .

The inversion mapping is defined by

$$\vec{\mathbf{r}} = \frac{R^2}{r^2} \vec{r} \quad (63)$$

Radial distances change under the inversion, $\mathbf{r} = R^2/r$, but angles do not, $\hat{\mathbf{r}} = \hat{\mathbf{r}}$. Under an inversion the Laplacian does *not* transform into a geometric factor multiplying just the Laplacian, *except when* $N = 2$. In other dimensions, the Laplacian mixes with the *scale operator* under an inversion, as follows.

$$\nabla_r^2 = \left(\frac{\mathbf{r}^2}{R^2} \right)^2 \left(\nabla_{\mathbf{r}}^2 + \frac{2(2-N)}{\mathbf{r}^2} D_{\mathbf{r}} \right), \quad D_{\mathbf{r}} = \vec{\mathbf{r}} \cdot \vec{\nabla}_{\mathbf{r}} \quad (64)$$

This statement may be understood by considering harmonic functions, upon noting that under inversions r effectively becomes $1/r$, and only when $N = 2$ do both r^l and r^{-l} appear as factors in harmonic functions. For other N the factors are r^l and r^{2-N-l} .

Moreover, G itself is *not* invariant under the inversion, *except when* $N = 2$. This is obvious on dimensional grounds, since $G(\vec{r}, 0) \propto 1/r^{N-2} \xrightarrow{\text{inversion}} \mathbf{r}^{N-2}/R^{2N-4} \propto (\mathbf{r}^{2N-4}/R^{2N-4}) G(\vec{\mathbf{r}}, 0)$. More precisely, in N spatial dimensions,

$$G(\vec{r}_1; \vec{r}_2) \xrightarrow{\text{inversion}} \frac{\mathbf{r}_1^{N-2} \mathbf{r}_2^{N-2}}{R^{2N-4}} G(\vec{\mathbf{r}}_1; \vec{\mathbf{r}}_2) \quad (65)$$

Note the symmetry under $\vec{r}_1 \leftrightarrow \vec{r}_2$ is maintained under $\vec{\mathbf{r}}_1 \leftrightarrow \vec{\mathbf{r}}_2$. The complete transformation of the differential equation for the Green function in N dimensions is

$$\nabla_{r_1}^2 G(\vec{r}_1; \vec{r}_2) = -\frac{1}{\sqrt{g}} \delta^N(\vec{r}_1 - \vec{r}_2) \xrightarrow{\text{inversion}} \quad (66)$$

$$\left(\frac{\mathbf{r}_1^2}{R^2} \right)^2 \left(\nabla_{\mathbf{r}_1}^2 + \frac{2(2-N)}{\mathbf{r}_1^2} D_{\mathbf{r}_1} \right) \left(\frac{\mathbf{r}_1^{N-2} \mathbf{r}_2^{N-2}}{R^{2N-4}} G(\vec{\mathbf{r}}_1; \vec{\mathbf{r}}_2) \right) = -\frac{\mathbf{r}_1^{N+1}}{R^{2N}} \delta(\mathbf{r}_1 - \mathbf{r}_2) \delta^{N-1}(\hat{\mathbf{r}}_1 - \hat{\mathbf{r}}_2) \quad (67)$$

Again the $N = 2$ case is especially simple. For $N = 2$, up to a common factor, the equation is unchanged in form by the inversion.

In view of these results, it is not difficult to map only the lower branch of the squashed wormhole into the interior of the hypersphere while leaving the upper branch unchanged, thereby obtaining a single copy of \mathbb{E}_N that includes both the exterior and the interior of the hypersphere. In the course of this inversion, the image charge is moved to its more conventional position within the hypersphere. We leave the details as an exercise for the reader.

8 On the grounded conducting disk in 3D

Hobson used Sommerfeld's method and a clever coordinate choice to find the Green function for an equipotential circular disk in three Euclidean dimensions [10]. In this approach, the disk serves as a doorway between two copies of \mathbb{E}_3 , with the unit source and field point located in one copy of \mathbb{E}_3 , and an equal strength, negative image of the source obviously placed in the same position as the source except in the second copy of \mathbb{E}_3 . Nearly forty years later, Waldmann (a student of Sommerfeld) offered another solution to this problem [16] by mapping the half-plane to a finite radius disk and then transforming Sommerfeld's 1897 result for the grounded half-plane Green function. Another thirty-four years after that, Davis and Reitz independently solved the same problem, again using Sommerfeld's method but with an emphasis on the use of complex analysis to construct directly the Green function on the two copies of \mathbb{E}_3 [3]. In this regard, their approach is more in line with Sommerfeld's original analysis, wherein complex variables also play a central role.

Neither of these treatments invoke Riemannian geometry as we have done here for hyperspheres. However it is possible in principle to consider the conducting disk in \mathbb{E}_3 as a squashed oblate spheroid, and thereby obtain the Green function for the disk by taking a limit of Green functions on branched manifolds connected by spheroidal generalizations of the Ellis wormhole, analogous to the p -norm wormholes used above. This more geometrical treatment will be discussed elsewhere [1].

9 Conclusions

We have obtained the Green function for grounded hyperspheres in N spatial dimensions by first constructing Green functions on Riemannian manifolds (rather unfortunately, in our opinion, but commonly known as “wormholes”) and then by squashing these manifolds to produce two copies of flat Euclidean space creased together along a hypersphere of radius R . The distribution of source and image charges on the final squashed manifold illustrates Sommerfeld’s generalization of Thomson’s method.

Sommerfeld knew that his generalized method could be used to solve a large variety of problems [15], writing to Klein in the spring of 1897 (see [6] page 80):

“The number of boundary value problems solvable by means of my elaborated Thomson’s method of images is very great.”

But he does not seem to have pursued this during the next half-century, perhaps because more interesting mathematics and physics questions captured his attention.

In our opinion, the most prescient aspect of Sommerfeld’s nineteenth century work lies in its suggestion that physical problems in electromagnetic theory may be simplified and perhaps more easily understood through the study of Riemannian geometries, a view that developed much later in general relativity. However, like Riemann before him, in 1897 Sommerfeld had no reason to include time along with the spatial dimensions of his envisioned manifolds, thus making his work premature.

Nevertheless, considering its application of Riemann’s ideas from geometry and complex analysis to higher dimensional branched manifolds, we believe Sommerfeld’s work should be recognized as a legitimate precursor to the wormhole studies that appeared a few decades later [9, 7, 8] and continue to the present day [14, 11, 12]. We hope our paper encourages readers to share this opinion.

Acknowledgements It has been our pleasure to reconsider this elementary subject during the year of the Feynman Centennial and the Sommerfeld Sesquicentennial. This work was supported in part by a University of Miami Cooper Fellowship, and by a Clark Way Harrison Visiting Professorship at Washington University in Saint Louis.

References

- [1] H Alshal and T Curtright, in preparation.
- [2] T Curtright, H Alshal, P Baral, S Huang, J Liu, K Tamang, X Zhang, and Y Zhang, “The Conducting Ring Viewed as a Wormhole” [<https://arxiv.org/abs/1805.11147>].
- [3] L C Davis and J R Reitz, “Solution to potential problems near a conducting semi-infinite sheet or conducting disc” Am. J. Phys. 39 (1971) 1255-1265.
- [4] L C Davis and J R Reitz, “Solution of potential problems near the corner of a conductor” J. Math. Phys. 16 (1975) 1219–1226.
- [5] D G Duffy, *Green’s Functions with Applications*, Second Edition, CRC Press (2017) ISBN-13: 978-1482251029.
- [6] M Eckert, *Arnold Sommerfeld: Science, Life and Turbulent Times 1868-1951*, Springer-Verlag (2013) ISBN-13: 978-1461474609.
- [7] A Einstein and N Rosen, “The Particle Problem in the General Theory of Relativity” Phys. Rev. 48 (1935) 73-77.
- [8] H G Ellis, “Ether flow through a drainhole: A particle model in general relativity” J. Math. Phys. 14 (1973) 104–118.
- [9] L Flamm, “Beiträge zur Einsteinschen Gravitationstheorie” Physikalische Zeitschrift 17 (1916) 448-454.

- [10] E. W. Hobson, “On Green’s function for a circular disc, with application to electrostatic problems” Trans. Cambridge Philos. Soc. 18 (1900) 277- 291.
- [11] O James, E von Tunzelmann, P Franklin, and K S Thorne, “Visualizing *Interstellar’s* Wormhole” Am. J. Phys. 83 (2015) 486-499 [<https://arxiv.org/abs/1502.03809>].
- [12] F S N Lobo (editor), *Wormholes, Warp Drives and Energy Conditions*, Springer-Verlag (2017) ISBN-13: 978-3319551814.
- [13] J Mehra, *The Beat of a Different Drum: The Life and Science of Richard Feynman*, Oxford University Press (1994) ISBN-13: 978-0198539483.
- [14] M S Morris and K S Thorne, “Wormholes in spacetime and their use for interstellar travel: A tool for teaching general relativity” Am. J. Phys. 56 (1988) 395-412.
- [15] A Sommerfeld, “Über verzweigte Potentiale im Raum” Proc. London Math. Soc. (1896) s1-28 (1): 395-429; ibid. 30 (1899) 161.
- [16] L Waldmann, “Zwei Anwendungen der Sommerfeld’schen Methode der verzweigten Potentiale” Physikalische Zeitschrift 38 (1937) 654–663.

Figures

The first nine Figures show equatorial surface slices of various p -norm wormholes, as embeddings in three dimensions, where

$$(ds)^2 = (dw)^2 + r^2(w) (d\theta)^2 = (dx)^2 + (dy)^2 + (dz)^2 \quad (\text{F1})$$

$$x(w, \theta) = r(w) \cos \theta, \quad y(w, \theta) = r(w) \sin \theta, \quad r(w) = \left(R^p + (w^2)^{p/2} \right)^{1/p} \quad (\text{F2})$$

$$z(w) = \int_0^w \sqrt{1 - (dr(\varpi)/d\varpi)^2} d\varpi = \int_0^w \sqrt{1 - (\varpi^2)^{p-1} \left(R^p + (\varpi^2)^{p/2} \right)^{\frac{2}{p}-2}} d\varpi \quad (\text{F3})$$

For example, for $p = 2$,

$$z(w) = R \ln \left(\frac{w + \sqrt{R^2 + w^2}}{R} \right) = R \operatorname{arcsinh} \left(\frac{w}{R} \right) \quad (\text{F4})$$

For generic p , it is easiest to obtain $z(w)$ by numerical solution of

$$\frac{dz(w)}{dw} = \sqrt{1 - (w^2)^{p-1} \left(R^p + (w^2)^{p/2} \right)^{\frac{2}{p}-2}} \quad (\text{F5})$$

with initial condition $z(0) = 0$.

Figures 1-9: Embedded p -norm wormhole equatorial surfaces for p as shown. All plots are for $R = 1$, with $0 \leq \theta \leq 2\pi$ and $-2 \leq w \leq 2$. Upper and lower branches of the surfaces are in orange and green, respectively.

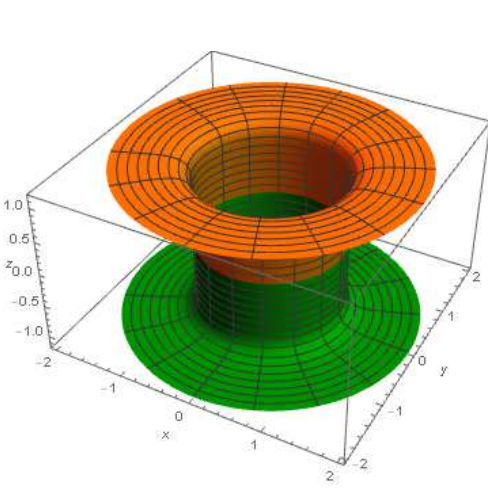


Figure 1: $p = 17$

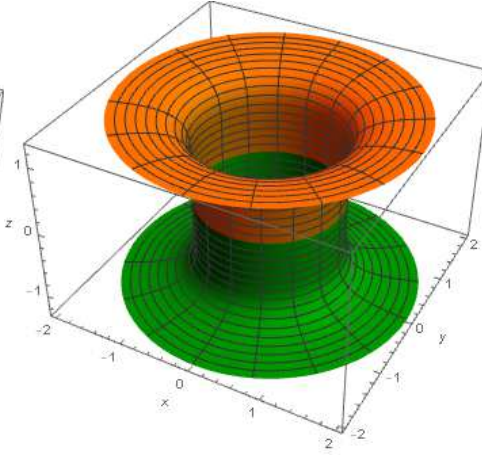


Figure 2: $p = 9$

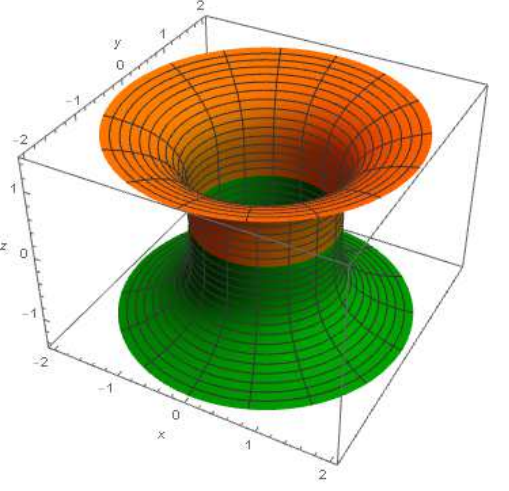


Figure 3: $p = 5$

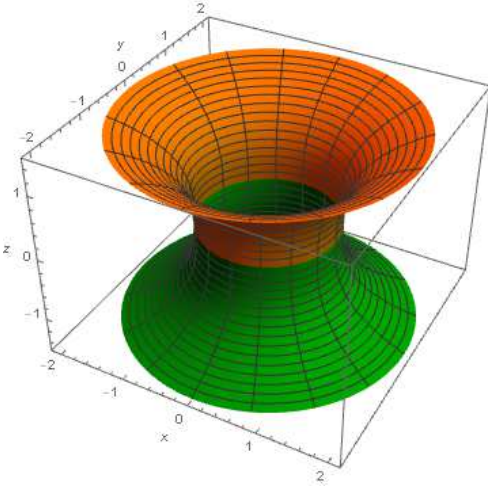


Figure 4: $p = 3$

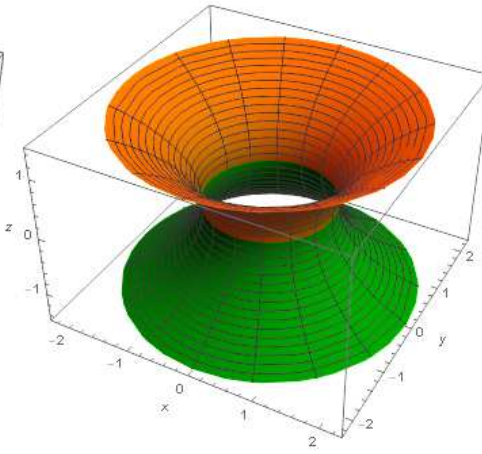


Figure 5: $p = 2$

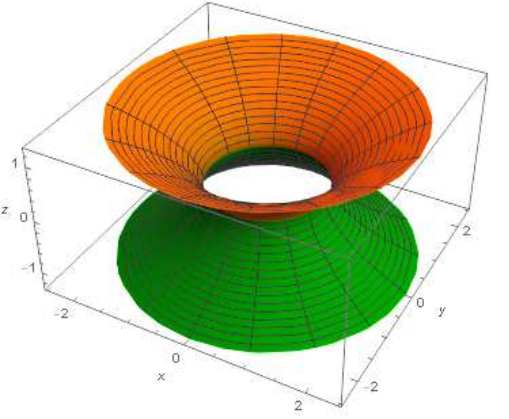


Figure 6: $p = 3/2$

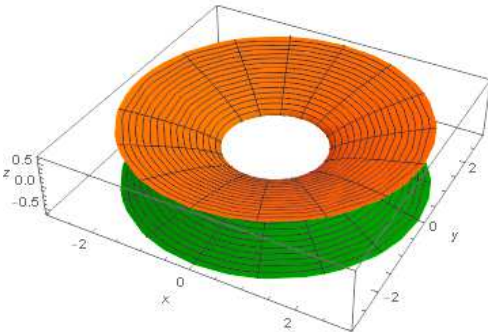


Figure 7: $p = 17/16$

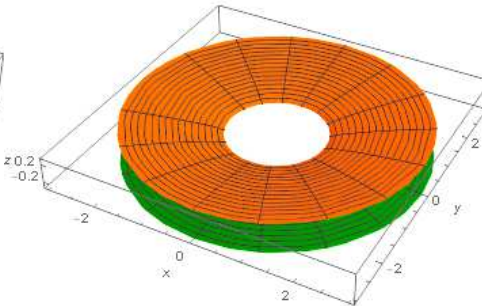


Figure 8: $p = 65/64$

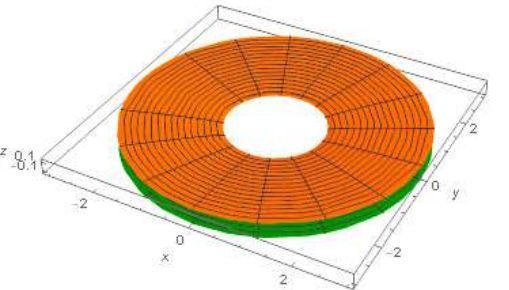


Figure 9: $p = 257/256$

The next four Figures show contour plots of various Green functions with $N = 4$ and $R = 1$, for $-\pi \leq \theta \leq \pi$ along the vertical axes, where $\theta \equiv \arccos(\hat{r}_1 \cdot \hat{r}_2)$, and for $-2.5 \leq w_1 \leq 2.5$ along the horizontal axes. The contours show $|G \text{ or } G_o| \leq 0.25$.

Figure 10: Plot of (47) versus w_1 and θ with source at $(w_2, \hat{r}_2) = (1, \hat{r}_2)$.

Figure 11: Plot of (28) using (47) with source at $(w_2, \hat{r}_2) = (1, \hat{r}_2)$ & image at $(-w_2, \hat{r}_2) = (-1, \hat{r}_2)$.

Figure 12: Plot of (55) and (57) for $N = 4$ versus w_1 and θ with source at $(w_2, \hat{r}_2) = (1, \hat{r}_2)$.

Figure 13: Plot of (59) and (60) for $N = 4$, with source at $(w_2, \hat{r}_2) = (1, \hat{r}_2)$ & image at $(-w_2, \hat{r}_2) = (-1, \hat{r}_2)$.

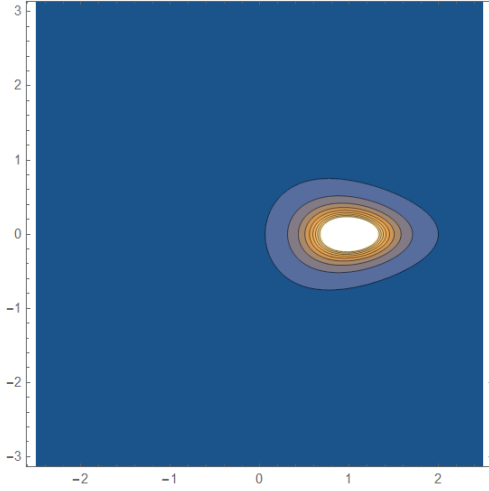


Figure 10: Contour plot of G for the Ellis wormhole in 4D.

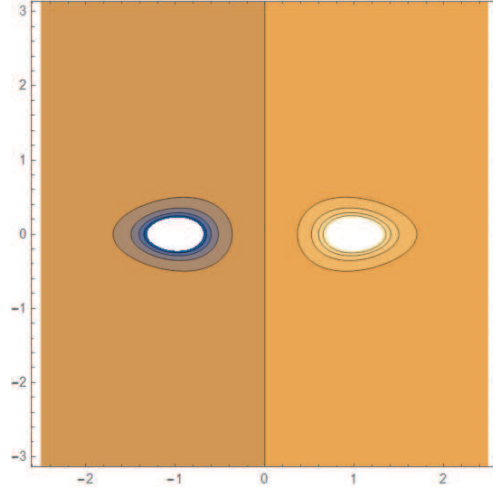


Figure 11: Contour plot of G_o for the Ellis wormhole in 4D.

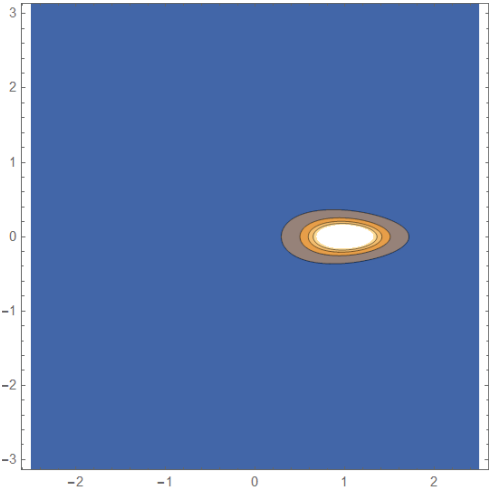


Figure 12: Contour plot of G for the squashed wormhole in 4D.

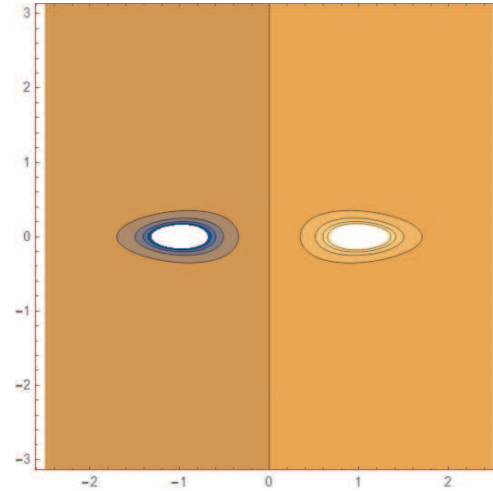


Figure 13: Contour plot of G_o for the squashed wormhole in 4D.